Inorg. Chem. **2007**, *46*, 4145–4157

Tetrakis(thiadiazole)porphyrazines. 5. Electrochemical and DFT/TDDFT Studies of the Free-Base Macrocycle and Its Mg^{II}, Zn^{II}, and Cu^{II} Complexes

Maria Pia Donzello,[†] Claudio Ercolani,*[,†] Karl M. Kadish,*[,§] Giampaolo Ricciardi,*[,#] Angela Rosa,*[,#] and Pavel A. Stuzhin[‡]

Dipartimento di Chimica, Università degli Studi di Roma "La Sapienza", P.le A. Moro 5, Roma I-00185, Italy, Department of Chemistry, University of Houston, Houston, Texas 77204-5003, Dipartimento di Chimica, Università della Basilicata, Via N. Sauro 85, I-85100 Potenza, Italy, and Ivanovo State University of Chemical Technology, Ivanovo 153460, Russia

Received January 10, 2007

The redox properties of the phthalocyanine-like tetrakis(thiadiazole)porphyrazines, [TTDPzM] (M = $Mg^{II}(H_2O)$, Zn^{II}, Cu^{II}, $2H^{I}$), were investigated by cyclic voltammetry, and their ground- and excited-state electronic properties were studied in detail by density functional theory (DFT) and time-dependent DFT (TDDFT) methods. Bulk and specific (axial ligation) solvent effects on the molecular and electronic structure were also taken into account. The title compounds show stepwise reversible ligand-centered one-electron reductions in the range 0 to −2.0 V vs SCE, with $E_{1/2}$ values being systematically less negative than corresponding reduction potentials for the same processes of the phthalocyanine (Pc) analogues. No electroxidations were observed at positive potentials. The observed redox behavior is rationalized on the basis of the ground-state electronic structures which reveal that replacement of the benzo rings of the Pc macrocycle by electron-withdrawing thiadiazole rings induces a large stabilization of both the HOMO and LUMOs in the investigated macrocycles. An excellent correlation is found between the first one-electron reduction potentials and the gas-phase LUMO energies along the series. The same sequence in the first reduction potentials is theoretically reproduced in pyridine, even if the Zn^{II} and Mg^{II} complexes are assumed to be in the axially ligated form, [TTDPzM(py)]. TDDFT calculations of the lowest excited states of the Zn^{II}, Mg^{II}, and Cu^{II} complexes in pyridine provide an accurate description of their UV–visible spectra. The calculated optical spectra for the free-base macrocycle in chlorobenzene and pyridine confirm previous data in that the thiadiazoleporphyrazine [$TTDPzH_2$] is mostly present in pyridine in its deprotonated form $[TTDPz]^{2-}$. DFT results, in keeping with electrochemical data, indicate, however, that in pyridine it is the neutral species [$TTDPzH_2$] being reduced instead of its deprotonated form $[TTDPz]^{2-}$.

Introduction

The phthalocyanines (see Chart 1A for the unsubstituted free-base, [PcH_2]) have been so far the most widely studied family of porphyrazines, the tetraazaanalogues of porphyrins.[1,2] A number of structural modifications are possible in the porphyrazines, one of which involves the annulated benzene rings of the phthalocyanine macrocycle being replaced by electron-attracting rings having incorporated appropriate heteroatoms such as N, S, or Se. These novel families of macrocycles, while approaching in many respects the phthalocyanine framework, can have distinct structural and electronic features as well as physicochemical properties which would be of interest in terms of applications. Until very recently, only a few classes of such macrocycles were known, mainly those with pyridine or pyrazine rings directly annulated to the central porphyrazine core.[2,3] However, in

* To whom correspondence should be addressed. E-mail: claudio.ercolani@uniroma1.it.
[†] Università degli Studi di Roma "La Sapienza".
[§] University of Houston.
[#] Università della Basilicata.
[‡] Ivanovo State University of Chemical Technology.

(1) *The Porphyrin Handbook*; Kadish, K. M., Smith, K. M., Guilard, R., Eds.; Academic Press: New York, 2003; Vols. 15−20.

(2) *Phthalocyanines: Properties and Applications*; Leznoff, C. C., Lever, A. B. P., Eds.; VCH Publishers, Inc.: New York, 1989−1996; Vols. 1−4.

10.1021/ic070038d CCC: $37.00
Published on Web 04/20/2007

Chart 1. Schematic Representation of the Structure of [PcH_2] (A), [$TTDPzH_2$] (B), and [$TSeDPzH_2$] (C)

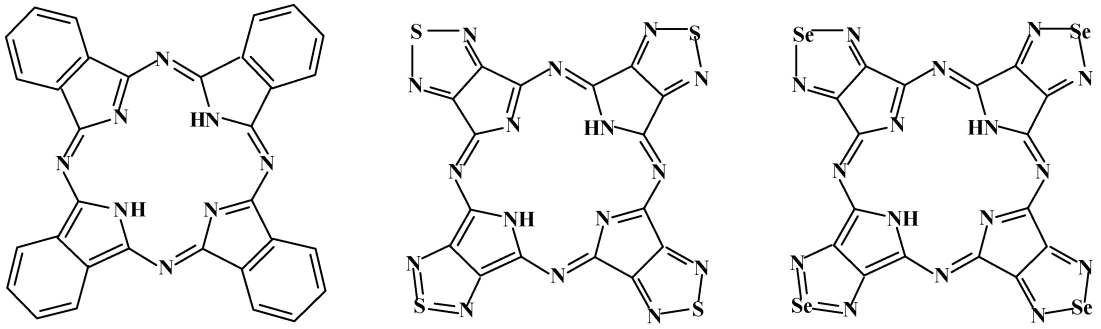

A B C

the past decade several classes of similarly substituted porphyrazines have been synthesized and their properties investigated by our laboratories.[4−7] These studies have shown that the presence of peripherally annulated highly electron-deficient heterocyclic rings in tetrakis(thia/selenodiazole)-porphyrazines,[4] tetrakis(diphenyldiazepino)porphyrazines,[5] and tetrakis(dipyridinopyrazino)porphyrazines[6] leads to a rearrangement of the electronic distribution within the porphyrazine framework as compared to that present in the phthalocyanine macrocycle, thus resulting in somewhat modified physicochemical behavior with implied differences in solid-state and/or solution properties.

A detailed electrochemical investigation was previously carried out for the series of tetrakis(diphenyldiazepino)-porphyrazines [Ph_8DzPzM] (M = $2H^I$, $Mg^{II}(H_2O)$, Zn^{II}, Cu^{II}, Co^{II}, Mn^{II})[5] as well as for the tetrakis(dipyridinopyrazino)-porphyrazines [$Py_8TPyzPzM$] (M = $2H^I$, $Mg^{II}(H_2O)$, Zn^{II}, Cu^{II}, Co^{II}, Mn^{II})[6] including their corresponding octacations [$(2\text{-Mepy})_8TPyzPzM]^{8+}$ (M = $2H^I$, $Mg^{II}(H_2O)$, Zn^{II}, Cu^{II}, Co^{II}).[7] Electrochemical studies were also reported for the "thiadiazoleporphyrazines" carrying tervalent metal ions and having the formula [TTDPzMX] where M = Al^{III}, Ga^{III}, In^{III} and X = Cl^-, Br^-, or CH_3COO^-.[8] Multistep reversible one-electron reduction processes were observed for all of the above species[5−8] over the cathodic range 0 → −2.0 V vs SCE in different nonaqueous solvents (pyridine, dimethylsulfoxide, dimethylformamide, and CH_2Cl_2). The electrode reactions were in almost all cases ligand-centered, with the single exception being the $Co^{II} \rightarrow Co^{I}$ process. From these studies it was shown that, due to the presence of the external electron-withdrawing fragments, the stepwise one-electron reductions occur at remarkably less negative potentials than for related reductions of phthalocyanine analogues having the same central metal ions. This means that the acceptance of electrons is significantly facilitated in the new porphyrazine systems. Moreover, the one-electron redox processes are for the most part reversible, which indicates that the excess charge on the compound after electroreduction is easily redistributed and stabilized within the entire macrocyclic framework as each negatively charged species is formed. The electronic structure changes induced by the peripheral highly electron-deficient fragments are also reflected in the electronic absorption spectra which exhibit a blue shift of the Q and B bands and a more complex B band region as compared to phthalocyanines with the same metal ions.

Based on the large amount of information available on these new families of porphyrazines, including synthetic and structural work as well as their general physicochemical properties,[4−8] it was thought to be of great interest to now attempt a theoretical investigation, based on DFT/TDDFT calculations, where we are able to elucidate the electronic origin of the peculiar electrochemical and optical behavior. It is emphasized here that such types of studies are in general only rarely encountered in the porphyrazine literature. In fact, to our knowledge, DFT calculations of the ground-state molecular and electronic structure have only been reported for a few metal derivatives (Ti^{IV}, V^{IV}, Zr^{IV}) of unsubstituted tetrapyrazinoporphyrazine[9] and for [$TTDPzH_2$].[10] For this latter species the lowest excited states have also been investigated at the TDDFT/B3LYP and ZINDO level of theory.[10,11]

Tetrakis(thiadiazole)porphyrazines [TTDPzM] (M = $Mg^{II}(H_2O)$, Zn^{II}, Cu^{II}, $2H^I$)[4a,b] were selected for the present study

(3) (a) Stuzhin, P. A.; Ercolani, C. *The Porphyrin Handbook*; Kadish, K. M., Smith, K. M., Guilard, R., Eds.; Academic Press: New York, 2003; Vol. 15, Chapter 101, pp 263−364. (b) Leznoff, C. C. In *Phthalocyanines − Properties and Applications*; Leznoff, C. C., Lever, A. B. P., Eds.; VCH Publishers, Inc.: New York, 1993; Vol.1, pp 2−54. (c) Kudrevich, S. V.; van Lier, J. E. *Coord. Chem. Rev.* **1996**, *156*, 163−182.

(4) (a) Stuzhin, P. A.; Bauer, E. M.; Ercolani, C. *Inorg. Chem*. **1998**, *37*, 1533. (b) Bauer, E. M.; Cardarilli, D.; Ercolani, C.; Stuzhin, P. A.; Russo, U. *Inorg. Chem.* **1999**, *38*, 6114. (c) Bauer, E. M.; Ercolani, C.; Galli, P.; Popkova, I. A.; Stuzhin, P. A. *J. Porphyrins Phthalocyanines* **1999**, *3*, 371. (d) Angeloni, S.; Bauer, E. M.; Ercolani, C.; Popkova, I. A.; Stuzhin, P. A. *J. Porphyrins Phthalocyanines* **2001**, *5*, 881.

(5) (a) Donzello, M. P.; Ercolani, C.; Stuzhin, P. A.; Chiesi-Villa, A.; Rizzoli, C. *Eur. J. Inorg. Chem*. **1999**, 2075. (b) Donzello, M. P.; Dini, D.; D'Arcangelo, G.; Ercolani, C.; Zhan, R.; Ou, Z.; Stuzhin, P. A.; Kadish, K. M. *J. Am. Chem. Soc.* **2003**, *125*, 14190.

(6) (a) Donzello, M. P.; Ou, Z.; Monacelli, F.; Ricciardi, G.; Rizzoli, C.; Ercolani, C.; Kadish, K. M. *Inorg. Chem.* **2004**, *43*, 8626. (b) Donzello, M. P.; Ou, Z.; Dini, D.; Meneghetti, M.; Ercolani, C.; Kadish, K. M. *Inorg. Chem.* **2004**, *43*, 8637.

(7) (a) Bergami, C.; Donzello, M. P.; Ercolani, C.; Monacelli, F.; Kadish, K. M.; Rizzoli, C. *Inorg. Chem*. **2005**, *44*, 9852. (b) Bergami, C.; Donzello, M. P.; Monacelli, F.; Ercolani, C.; Kadish, K. M. *Inorg. Chem*. **2005**, *44*, 9862.

(8) Donzello, M. P.; Agostinetto, R.; Ivanova, S. S.; Fujimori, M.; Suzuki, Y.; Yoshikawa, H.; Shen, J.; Awaga, K.; Ercolani, C.; Kadish, K. M.; Stuzhin, P. A. *Inorg. Chem.* **2005**, *44*, 8539.

(9) Dini, D.; Hanack, M.; Egelhaaf, H.-J.; Snache-Garcia, J. C.; Cornil, J. *J. Phys. Chem. B* **2005**, *109*, 5425.

(10) Zhou, X.; Ren, A.-M.; Feng, J-K.; Shuai, Z. *J. Photochem. Photobiol., A* **2005**, *172*, 126.

since these species, which have been the subject of a recent review together with their Se analogues (see, respectively, parts B and C of Chart 1 for the unmetalated species),[12] are in many respects (square planar molecular structure, extended π-conjugation, low solubility, thermal stability and sublimability) the class of porphyrazines which most closely resemble the phthalocyanines. Electrochemical studies of the above [TTDPzM] series of compounds in coordinating and noncoordinating nonaqueous solvents are presented for the first time in the current paper together with a detailed DFT/TDDFT investigation of their ground- and excited-state properties, both in the gas phase and in solution. Special emphasis is given to the electronic origin of the particular electrochemical and spectroscopic behavior of these systems relative to their phthalocyanine analogues.

Experimental Section

The tetrakis(thiadiazole)porphyrazines, represented as [TTDPzM] (M = $Mg^{II}(H_2O)$, Zn^{II}, Cu^{II}, $2H^{I}$) were prepared as previously reported.[4a,b] All of the compounds normally contain some additional clathrated water (1 or 2 mol per mol of macrocycle) after exposure to air. The amount of the water present is not rigorously defined and depends upon the specific sample and the ambient conditions.[4] The water molecules were not expected (nor shown) to influence the electrochemistry of these materials in nonaqueous media, and the presence of water is therefore neglected in the given formulation of each compound.

Electrochemical Measurements. Cyclic voltammetry (CV) measurements were performed at 298 K using an EG&G model 173 potentiostat coupled with an EG&E model 175 universal programmer. Measurements were made in pyridine (Aldrich, anhydrous, 99.8%), dimethylsulfoxide (DMSO; Aldrich, anhydrous, 99.8%), and dimethylformamide (DMF; Aldrich, anhydrous, 99.8%) containing 0.1 M tetrabutylammonium perchlorate (TBAP) as supporting electrolyte. High purity N_2 from Trigas was used to deoxygenate the solution before each electrochemical experiment. TBAP was purchased from Sigma Chemical or Fluka Chemika Co., recrystallized from ethyl alcohol, and dried under vacuum at 40 °C for at least one week prior to use. A three-electrode system was used and consisted of a glassy carbon working electrode, a platinum wire counter electrode, and a saturated calomel reference electrode (SCE). The reference electrode was separated from the bulk of the solution by a fritted-glass bridge filled with the solvent/supporting electrolyte mixture.

Computational Details. All calculations reported in this paper were performed with the Amsterdam Density Functional (ADF) package, release 2006.01.[13,14] Geometry optimizations were carried out at the BP86 level of DFT.[15,16] The optimized structures were verified to be true minima by frequency calculations.

Excitation energies and oscillator strengths were computed using TDDFT methods.[17−20] Ground- and excited-state calculations at the optimized geometries were done using the model Kohn−Sham exchange-correlation potential SAOP.[21] This potential has been successfully used in ground- and excited-state calculations of metallotetrapyrroles.[22] In all of the DFT and TDDFT calculations, the all-electron ADF TZ2P basis set, which is an uncontracted triple-ζ STO basis with two polarization functions, was used. Since the electrochemical and optical properties of the title compounds were investigated in solution, the calculations have also taken into account bulk solvent effects using the "Conductor-like Screening Model" (COSMO)[23] as implemented in ADF[24] and by using pyridine and chlorobenzene (PhCl) (in the case of [$TTDPzH_2$]) as solvents.

Results and Discussion

Electrochemical Behavior. Cyclic voltammetry (CV) was used to measure the redox potentials of [TTDPzM] in pyridine, DMSO, and DMF solutions. Electrochemical measurements could not be carried out in the nondonor solvents CH_2Cl_2 or PhCl owing to a low solubility of the compounds under these solution conditions, and only qualitative UV−visible spectra could be measured in these solvents.[4a,b]

A cyclic voltammogram of [TTDPzCu] in pyridine containing 0.1 M TBAP is illustrated in Figure 1(top). The compound exhibits four reversible and well separated one-electron reductions at $E_{1/2}$ = −0.29, −0.81, −1.46, and −1.92 V vs SCE. Similar electrochemical behavior in the same solvent is seen (Figure 1) for the Mg^{II} and Zn^{II} analogues as well as for the unmetalated macrocycle [TTDPzH$_2$], although the fourth reduction could not be easily seen in all cases due to its proximity to the negative potential limit of the solvent. No oxidations were observed for any of the four compounds at positive potentials up to +1.0 V vs SCE. The cyclic voltammetric response, similar to that in pyridine, is shown for DMSO in Figure S1 (Supporting Information).

Table 1 lists the half-wave potentials ($E_{1/2}$, V vs SCE) for reduction of the [TTDPzM] derivatives in pyridine, DMSO, and DMF. The potential separations between each two sequential reductions are also given in this table, labeled as Δ_{1-2}, Δ_{2-3}, and Δ_{3-4}. For each reduction there is only a slight solvent dependence on $E_{1/2}$ between pyridine and DMSO.

(11) (a) Stuzhin, P. A. Ph.D. Dissertation, Ivanovo, 2004; 383 pp. (b) Stuzhin, P. A.; Ercolani, C. Symposium Lecture ICPP3. *J. Porphyrins Phthalocyanines* **2004**, *8*, 495.
(12) Donzello, M. P.; Ercolani, C.; Stuzhin, P. A. *Coord. Chem. Rev.* **2006**, *250*, pp. 1530−1561.
(13) *ADF: Density Functional Theory* (*DFT*) *Software for Chemists*; Scientific Computing & Modelling: Amsterdam. http://www.scm.com (accessed 2006).
(14) te Velde, G.; Bickelhaupt, F. M.; Baerends, E. J.; Fonseca Guerra, C.; van Gisbergen, S. J. A.; Snijders, J. G.; Ziegler, T. *J. Comput. Chem.* **2001**, *22*, 931.
(15) Becke, A. *Phys. Rev. A* **1988**, *38*, 3098.
(16) Perdew, J. P. *Phys. Rev. B* **1986**, *33*, 8822 (Erratum: PRB 34 **1986**, 7406).
(17) Gross, E. K. U.; Kohn, W. *Adv. Quantum Chem.* **1990**, *21*, 255.
(18) Gross, E. U. K.; Dobson, J. F.; Petersilka, M. Density Functional Theory. In *Springer Series "Topics in Current Chemistry"*; Nalewajski, R. F., Ed.; Springer: Heidelberg, 1996.
(19) Casida, M. E. In *Recent Advances in Density Functional Methods*; Chong, D. P., Ed.; World Scientific: Singapore, 1995; Vol. 1, p 155.
(20) Bauernschmitt, R.; Ahlrichs, R. *J. Chem. Phys.* **1996**, *104*, 9047.
(21) (a) Gritsenko, O. V.; Schipper, P. R. T.; Baerends, E. J. *Chem. Phys. Lett.* **1999**, *302*, 199. (b) Schipper, P. R. T.; Gritsenko, O. V.; van Gisbergen, S. J. A.; Baerends, E. J. *J. Chem. Phys.* **2000**, *112*, 1344.
(22) (a) Rosa, A.; Ricciardi, G.; Baerends, E. J.; van Gisbergen, S. J. A. *J. Phys. Chem. A* **2001**, *112*, 1344. (b) Ricciardi, G.; Rosa, A.; Baerends, E. J. *J. Phys. Chem.* **2001**, *105*, 5242. (c) Baerends, E. J.; Ricciardi, G.; Rosa, A.; van Gisbergen, S. J. A. *Coord. Chem. Rev.* **2002**, *230*, 5. (d) Rosa, A.; Ricciardi, G.; Gritsenko, O.; Baerends, E. J. *Struct. Bonding (Berlin)* **2004**, *112*, 49.
(23) (a) Klamt, A.; Schürmann, G. *J. Chem. Soc., Perkin Trans.* **1993**, *2*, 799. (b) Klamt, A.; Jonas, V. *J. Chem. Phys.* **1996**, *105*, 9972.
(24) Pye, C. C.; Ziegler, T. *Theor. Chem. Acc.* **1999**, *101*, 396.

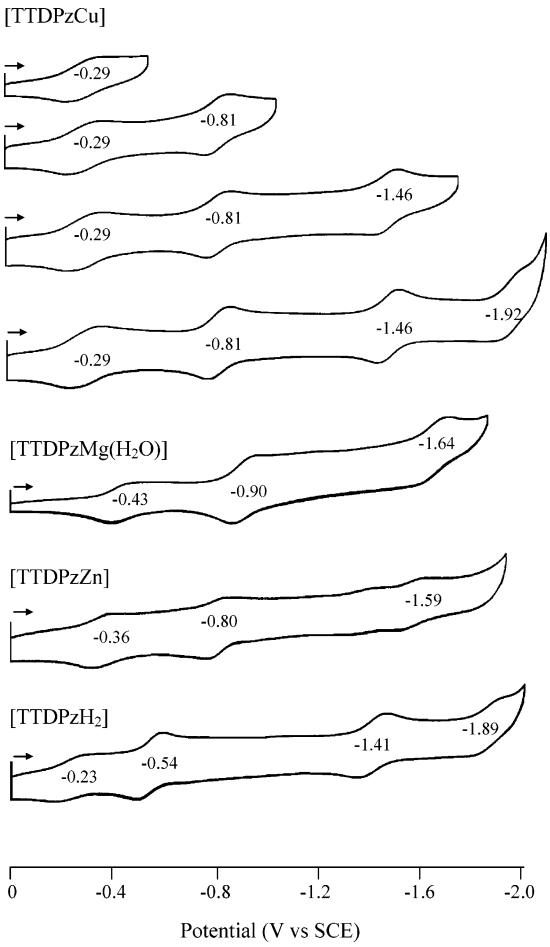

Figure 1. Cyclic voltammograms, with added $E_{1/2}$ values of [TTDPzM] and [TTDPzH$_2$] compounds in pyridine (second scan); 0.1 M TBAP, scan rate = 100 mV/s.

Similar values of Δ_{1-2}, Δ_{2-3}, and Δ_{3-4} are also found in the two solvents with the values in most cases differing by no more than 30 mV, the only exceptions being for the first reduction of the Mg^{II} and Cu^{II} complexes where large variations are observed (see Table 1). This result indicates that identical stepwise reduction processes must take place in the two solvents. Data roughly in line with those obtained in pyridine and DMSO were also observed in DMF for the Zn^{II} and Cu^{II} complexes (Table 1).

The sequence of the reduction processes involving the $[TTDzPzM]^{0\rightarrow1\rightarrow2\rightarrow3\rightarrow4-}$ couples are given in eqs 1−4 for M = $Mg^{II}(H_2O)$, Zn^{II}, and Cu^{II}. Each of the four reductions are ligand-centered, independent of the central metal ion. However, before discussing these data for the metal derivatives, it is appropriate to describe in more detail the cyclic voltammetric behavior of the free-base porphyrazine.

$$[TTDPzM] + e^- \leftrightarrows [TTDPzM]^- \quad (1)$$

$$[TTDPzM]^- + e^- \leftrightarrows [TTDPzM]^{2-} \quad (2)$$

$$[TTDPzM]^{2-} + e^- \leftrightarrows [TTDPzM]^{3-} \quad (3)$$

$$[TTDPzM]^{3-} + e^- \leftrightarrows [TTDPzM]^{4-} \quad (4)$$

The UV−visible spectrum of 10^{-5} M [TTDPzH$_2$] in pyridine indicates that the macrocycle is preponderantly in its deprotonated form, $[TTDPz]^{2-}$, as clearly supported by the presence of an unsplit Q band, thus suggesting D_{4h} symmetry.[4a] As indicated above, the cyclic voltammograms of [TTDPzH$_2$] in pyridine closely resemble voltammograms of the related metal complexes [TTDPzM]. In fact, four well-resolved one-electron reductions can be seen in pyridine (Figure 1) at $E_{1/2} = -0.23$, -0.54, -1.41, and -1.89 V. It might be reasonably assumed here that these values are assigned to reductions of the neutral species which undergoes a stepwise series of one-electron additions giving $[TTDPzH_2]^{0\rightarrow1\rightarrow2\rightarrow3\rightarrow4-}$. However, the spectroscopic data show that the deprotonated anion $[TTDPz]^{2-}$ is largely present in pyridine solution,[4a] and prior to reduction this dianion rapidly transforms into the neutral free-base porphyrazine through the equilibrium given in eq 5 after which the uncharged [TTDPzH$_2$] species is stepwise reduced in four one-electron-transfer processes. This conclusion is consistent with the fact that the dinegatively charged $[TTDPz]^{2-}$ should be much less easily reduced than the neutral species, with associated reduction potentials for all redox processes being shifted to $E_{1/2}$ values markedly more negative than for reduction of the corresponding neutral metal complexes (Table 1).

$$[TTDPz]^{2-} + 2H^+ \leftrightarrows [TTDPzH_2] \quad (5)$$

Further support for [TTDPzH$_2$] being reduced instead of $[TTDPz]^{2-}$ is given by data on the porphyrazine analogue "octapyridinotetrapyrazinoporphyrazine" [Py$_8$TPyzPzH$_2$] for which cyclic voltammetry in pyridine evidenced the presence of five ligand-centered redox processes.[6a] Four of these processes, with $E_{1/2} = -0.17$, -0.48, -1.24, and -1.61 V, values close to those given above for [TTDPzH$_2$], were assigned to the sequence of reductions $[Py_8TPyzPzH_2]^{0\rightarrow1\rightarrow2\rightarrow3\rightarrow4-}$.[6a] The remaining fifth reduction found at -0.93 V was assigned to a process involving the dianion $[Py_8TPyzPz]^{2-}$ as shown in eq 6.

$$[Py_8TPyzPz]^{2-} + e^- \leftrightarrows [Py_8TPyzPz]^{3-} \quad (6)$$

As can be seen from Table 1, potentials for the first reduction of the [TTDPzM] series of compounds in pyridine become progressively less negative in the sequence: Mg^{II} < Zn^{II} < Cu^{II} < $2H^I$ (-0.43, -0.36, -0.29, and -0.23 V vs SCE), a trend which is basically maintained for each reduction process of the same series of compounds. A well-defined set of electrochemical data has been published on a related series of macrocycles examined in our laboratory, namely "diazepinoporphyrazines" ([Ph$_8$DzPzM]),[5b] "pyrazinoporphyrazines" ([Py$_8$TPyzPzM]),[6] and their octacationic derivatives ([(2-Mepy)$_8$TPyzPzM]$^{8+}$)[7] plus a series of their

(25) (a) Clack, D. W.; Hosh, N. S.; Woosley, I. S. *Inorg. Chim. Acta* **1976**, *19*, 129. (b) Lever, A. B. P.; Wilshire, J. P. *Can. J. Chem.* **1976**, *54*, 2514.

Table 1. Half-Wave Potentials ($E_{1/2}$, V vs SCE) for Reduction of [TTDPzM] (M = $Mg^{II}(H_2O)$, Zn^{II}, Cu^{II}, $2H^{I}$) and [TTDPzMCl] (M = Al^{III}, Ga^{III}) in Pyridine, DMSO, or DMF Containing 0.1 M TBAP[a]

		reduction				$\Delta E_{1/2}$			
compound	solvent	first	second	third	fourth	Δ_{1-2}	Δ_{2-3}	Δ_{3-4}	ref
[TTDPzMg(H_2O)]	py	−0.43	−0.90	−1.64		0.47	0.74		tw[b]
	DMSO	−0.48	−0.87	−1.60	−2.06	0.39	0.73	0.46	tw[b]
[TTDPzZn]	py	−0.36	−0.80	−1.59		0.44	0.79		tw[b]
	DMSO	−0.44	−0.80	−1.58	−1.92	0.36	0.78	0.34	tw[b]
	DMF	−0.44	−0.87	−1.65		0.43	0.78		tw[b]
[TTDPzCu]	py	−0.29	−0.81	−1.46	−1.92	0.52	0.65	0.46	tw[b]
	DMSO	−0.37	−0.78	−1.40	−1.87	0.41	0.62	0.47	tw[b]
	DMF	−0.33	−0.75	−1.45		0.42	0.70		tw[b]
[TTDPzH_2]	py	−0.23	−0.54	−1.41	−1.87	0.31	0.87	0.46	tw[b]
	DMSO	−0.19	−0.51	−1.38	−1.82	0.32	0.87	0.44	tw[b]
[TTDPzAlCl]	py	−0.07	−0.54			0.47			8
	DMF	−0.10	−0.54			0.44			8
[TTDPzGaCl]	py	−0.13							8

[a] Scan rate = 100 mV/s. [b] tw = this work.

phthalocyanine analogues, [PcM].[25] A comparison of these data shows that the ordering of $E_{1/2}$ values with change of central metal ion is invariably the same for all reduction steps no matter which solvent is utilized. From the same set of data it also appears that the nature of the different peripheral substituents annulated to the central porphyrazine core will significantly affect the $E_{1/2}$ values for each specific level of reduction, i.e., the first, the second, etc. This is seen, for example, by comparing the sequence of $E_{1/2}$ values (V vs SCE) for the first reduction of the Zn^{II} complexes in pyridine. The sequence of $E_{1/2}$ values is as follows: −0.89 V ([PcZn]);[25b] identical to the value in DMF[25a]) < −0.72 V ([Ph_8DzPzZn])[5b] < −0.52 V ([TSeDPzZn])[26] < −0.36 V ([TTDPzZn], Table 1) < −0.34 V ([Py_8TPyzPzZn])[6b] < −0.26 V ([(2-Mepy)$_8$TPyzPzZn]$^{8+}$).[7b]

In a recent report,[8] the electrochemical behavior of complexes having the formula [TTDPzMX] (M = Al^{III}, Ga^{III}) and derived from the presently examined TTDPz macrocycle was studied. Noticeably, the $E_{1/2}$ values for first reduction of these tervalent complexes [TTDPzAlCl] and [TTDPzGaCl] in pyridine in DMF (−0.13 to −0.07 V) (Table 1) are at the less negative limit of the range of values measured for the series of compounds given above. They are also less negative than the first reduction potentials of all other [TTDPzM] complexes in pyridine (−0.43 to −0.23 V) or in DMSO (−0.48 to −0.19 V). X-ray analysis indicates that the two isostructural complexes [TTDPzAlCl] and [TTDPzGaCl] have a five-coordinate square pyramidal arrangement in the solid state with Al^{III} and Ga^{III} located at distances of 0.416(6) and 0.448(6) Å from the center of the N_4 chromophoric system, the Cl^- ion occupying the apical position (Al−Cl = 2.171(5) and Ga−Cl = 2.205(5) Å). The out-of-plane displacement of the metal centers in these two compounds and their lower electronegativity with respect to that of the bivalent metal ions in the [TTDPzM] series of complexes evidently favor the uptake of electrons, leading to formation of the negatively charged species. These findings parallel earlier results seen in pyridine for the phthalocyanine analogues, for which $E_{1/2}$ values for reduction of the tervalent complexes, i.e., [PcAlCl] and [PcGaCl], are less negative, −0.55 and −0.53 V,[8] respectively, than the range of values for reduction of the divalent [PcM] complexes (−0.91 to −0.66 V, DMF).[25a]

Quantum Chemical Calculations. In this section the ground-state molecular and electronic structure and the optical spectra of [TTDPzM] (M = Mg^{II}, Zn^{II}, Cu^{II}, $2H^{I}$) are computed, both in the gas phase and in solution, using DFT/TDDFT methods. These studies lead to a rationalization of the redox behavior of the investigated compounds and to an unambiguous interpretation of their optical spectra.

Molecular Structure. The X-ray crystal and molecular structure of free-base [TTDPzH_2] and its Cu^{II} and Zn^{II} complexes have recently been reported.[27] According to the experimental data, the "thiadiazoleporphyrazine" macrocycle is substantially planar in all three species. While the Cu^{II} ion lies in the plane of the macrocycle, the Zn^{II} ion is significantly displaced out of the central N_4 plane (0.394 Å). The out-of-plane displacement of the Zn^{II} ion was ascribed[27a] to a coordination interaction between the metal and a thiadiazole nitrogen (N_t) of a proximate macrocycle. Geometry optimization of [TTDPzH_2] and its Mg^{II}, Cu^{II}, and Zn^{II} derivatives was performed in the gas phase and in pyridine solution. The most relevant geometrical parameters calculated in the gas phase are summarized in Table 2 together with the available X-ray data.[27] The coordinate system used in the calculations and the labeling of the nonequivalent atomic centers are shown in Chart 2.

The present DFT/BP86 results, in agreement with previous DFT/B3LYP results,[10] predict a planar structure for [TTDPzH_2] with D_{2h} symmetry. As to the metal complexes, geometry optimization of structures of C_{4v} symmetry, with the metal atom displaced out of the plane of the macrocycle, invariably converged to D_{4h} structures. This indicates that the out-of-plane displacement of the metal ion observed in the crystal structure of [TTDPzZn][27a] is not dictated by intrinsic electronic factors, rather it is driven by intermolecular interactions, as already suggested by the X-ray work.[27a]

(26) Donzello, M. P., unpublished results.

(27) (a) Fujimori, M.; Suzuki, Y.; Yoshikawa, H.; Awaga, K. *Angew. Chem.* **2003**, *115*, 6043. (b) Suzuki, Y.; Fujimori, M.; Yoshikawa, H.; Awaga, K. *Chem. Eur. J.* **2004**, *10*, 5158.

Table 2. Selected Bond Distances (Å) and Bond Angles (deg) Calculated for [TTDPzM] (M = $2H^{I}$, Mg^{II}, Zn^{II}, Cu^{II})[a]

	[TTDPzH$_2$][b]	[TTDPzMg]	[TTDPzZn]	[TTDPzCu]
M−N$_p$		2.030	2.022	1.987
			2.043(5)	*1.984(5)*
C$_\alpha$−N$_p$	1.389/1.375	1.384	1.384	1.385
	1.382(2)/1.371(2)		*1.380(7)*	*1.381(7)*
C$_\alpha$−C$_\beta$	1.452/1.464	1.460	1.459	1.456
	1.447(3)/1.465(3)		*1.456(8)*	*1.451(8)*
C$_\beta$−C$_\beta$	1.428/1.419	1.427	1.425	1.419
	1.408(2)/1.400(3)		*1.408(8)*	*1.422(8)*
C$_\alpha$−N$_b$	1.312/1.330	1.326	1.323	1.318
	1.311(2)/1.331(2)		*1.326(7)*	*1.322(7)*
C$_\beta$−N$_t$	1.330/1.327	1.328	1.328	1.329
	1.329(3)/1.326(2)		*1.327(7)*	*1.325(7)*
S−N$_t$	1.646/1.655	1.650	1.650	1.651
	1.630(2)/1.646(2)		*1.641(5)*	*1.645(5)*
C$_\alpha$−N$_p$−C$_\alpha$	114.5/108.8	111.4	111.3	110.3
	113.6(2)/108.7(2)		*110.6(5)*	*110.3(4)*
C$_\alpha$−N$_b$−C$_\alpha$	124.7	125.5	125.1	123.5
	123.5(2)		*124.2(5)*	*122.7(5)*
N$_t$−S−N$_t$	101.4/100.9	101.1	101.1	101.2
	101.3(9)/100.5(8)		*100.7(3)*	*100.4(2)*

[a] X-ray data for [TTDPzH$_2$] (from ref 27a), [TTDPzZn] (from ref 27a), and [TTDPzCu] from (ref 27b) are in italics. [b] The data refer to pyrrole/pyrrolenine rings.

Chart 2. Atom Labeling Scheme for [PcM] (Left Side) and [TTDPzM] (Right Side)[a]

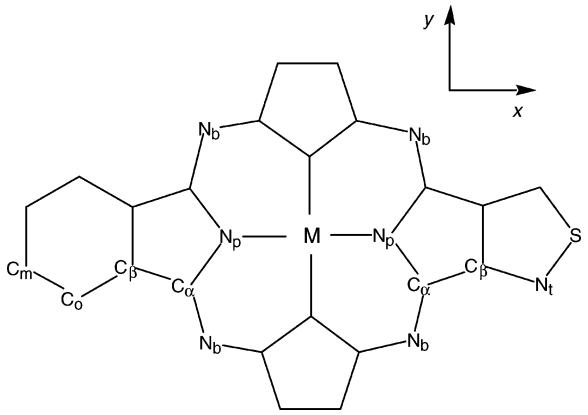

[a] In [TTDPzH$_2$] the two inner hydrogen atoms lie on the *x*-axis.

Excellent agreement is seen between the theoretical and experimental data. In particular, the calculated gas-phase structures nicely reproduce the effect of expansion of the porphyrazine core observed upon going from benzoporphyrazines (phthalocyanines) to thiadiazoleporphyrazines, a feature that has been widely discussed in a recent review.[12] The only discrepancy between theory and experiment concerns the Zn−N$_p$ distance, which is predicted to be somewhat shorter (~0.02 Å) than the experimental value on account of the in-plane location of the Zn^{II} ion in the calculated gas-phase structure. According to the data in Table 2, the macrocycle backbone of the alkaline earth complex—no structural data are available for [TTDPzMg] or its monohydrated derivative [TTDPzMg(H$_2$O)]—does not differ substantially from that of the transition-metal complexes [TTDPzCu] and [TTDPzZn].

Bulk solvent effects on the predicted geometries of the Cu^{II} and Zn^{II} complexes prove to be almost negligible, leading to changes in bond lengths and bond angles of less than 0.005 Å and 1°, respectively (compare data in Tables S1 and 2). However, specific interactions of the solvent with the investigated molecules must also be considered in order to fully characterize the species in solution.

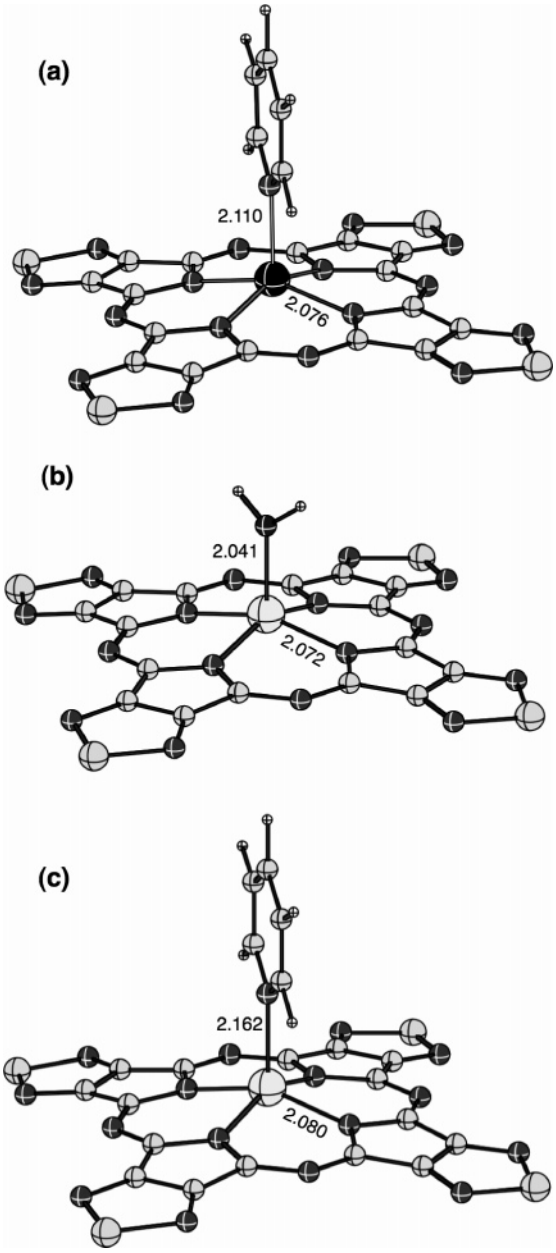

Figure 2. DFT-calculated structures in pyridine of [TTDPzZn(py)] (a), [TTDPzMg(H$_2$O)] (b), and [TTDPzMg(py)] (c). Selected bond distances (in Å) and angles (in deg) are shown.

As pointed out earlier, [TTDPzH$_2$] in pyridine is mostly present in its deprotonated form, $[TTDPz]^{2-}$. Thus, a structural characterization of this dianionic species was deemed to be necessary. Geometry optimization of the free-base dianion in pyridine afforded a structure with D_{4h} symmetry. The hole size of the macrocycle, i.e., the distance of the pyrrole N atoms from the center of the macrocycle cavity, is in $[TTDPz]^{2-}$ comparable to that computed for the Zn^{II} and Mg^{II} complexes in pyridine (2.009 Å vs 2.027 Å and 2.033 Å), although the macrocycle backbone shows sizable geometrical changes (see Table S1). These changes mainly consist of a shortening by ~0.02 Å in the C$_\alpha$−N$_p$

distance and a nearly comparable elongation of the remaining bonds which define the thiadiazolepyrrole moieties.

As noted above, effective interactions between the Zn^{II} ion and the thiadiazole N atom of a proximate macrocycle have been shown to exist in the crystal structure of [TTDPzZn].[27a] This suggests that the complex is likely to axially bind a solvent molecule in pyridine solution. To verify this point, the binding energy of an axially ligated pyridine molecule, E_{bind}(py), which is defined as the energy required (eq 7) to pull apart the axial ligand from the complex, was computed, taking the solution (pyridine) optimized ground-state structures of [TTDPzZn], py, and [TTDPzZn(py)].

$$-E_{bind}(py) = E([TTDPzZn(py)]) - \{E([TTDPzZn]) + E(py)\} \quad (7)$$

A value of 2.6 kcal/mol (without vibrational zero-point corrections) was computed for E_{bind}(py) suggesting that in pyridine solutions the zinc complex might also exist in its axially ligated form. Ligation of a second pyridine molecule to [TTDPzZn(py)], yielding the hexacoordinated [TTDPzZn-$(py)_2$] complex, is, instead, not likely to occur, as it is predicted to be endothermic by 4.6 kcal/mol. The pentacoordinated complex, [TTDPzZn(py)], is predicted to possess a slightly domed C_{2v} structure (see Figure 2a) in its $^1A_1$ ground-state. The axial ligation induces a considerable displacement of the metal out of the $(N_p)_4$ plane (0.467 Å) leading to elongation of the $Zn-N_p$ distance relative to the unligated parent complex (2.076 Å vs 2.022 Å). Interestingly, the calculated $Zn-N_{py}$ distance is very close to the $Zn-N_t$ distance measured in the crystal structure of [TTDPzZn] (2.110 Å vs 2.188 Å).

In a similar manner, the Mg^{II} complex is known to bear an axial water molecule in the solid state, so whether the water molecule is retained in pyridine solution or replaced by a solvent molecule is worthwhile to ascertain. To this end, the binding energy of both water and pyridine, has also been computed. The 10.2 kcal/mol and 11.6 kcal/mol values (without vibrational zero-point corrections) calculated for $E_{bind}(H_2O)$ and E_{bind}(py), respectively, suggest that the replacement of water by pyridine is an energetically favorable process. As pyridine is present in large excess, it is reasonable to assume that the magnesium complex is mostly present in pyridine solution as [TTDPzMg(py)]. The slightly domed structures of C_s and C_{2v} symmetry calculated for [TTDPzMg-(H_2O)] and [TTDPzMg(py)], respectively, are displayed in parts b and c of Figure 2.

Electronic Structure. The salient features of the electronic structure of the TTDPz macrocycle can be easily understood from the diagram of Figure 3 where the highest occupied and lowest unoccupied one-electron levels of [TTDPzZn] are compared to those of [PcZn], a phthalocyanine whose electronic structure has been investigated in detail, both experimentally[28] and theoretically.[22b,29]

The level scheme of Figure 3 shows that the most significant effect of replacing the benzo rings by thiadiazole rings is a large stabilization of all levels due to the higher electronegativity of the latter groups. For instance, upon going from [PcZn] to [TTDPzZn], the $1a_{1u}$-HOMO is stabilized by 1.21 eV. Actually, the $1a_{1u}$ level in [TTDPzZn] is even lower than in the parent [PzZn] (Pz = porphyrazine) (−10.07 vs −9.70[22c] eV), in spite of the antibonding with the annulated thiadiazole groups which is seen in the plot of Figure 3.

In both Zn^{II} complexes, a large energy gap separates the HOMO from the set of lower lying occupied orbitals, which comprise, in addition to the macrocycle π levels—the $1b_{2u}$, $1e_g$, $1a_{2u}$, and $2a_{2u}$—the in-plane levels associated with N_p lone pairs (the $1b_{1g}$) and N_b lone pairs (the $1b_{2g}$ and $1e_u$). The $1b_{1g}$ MO is pushed up by antibonding with the Zn-$3d_{x^2-y^2}$ that contributes to this orbital by ∼10% and becomes the HOMO-1. Actually, the $3d_{x^2-y^2}$ is the only 3d orbital which interacts to some extent with the macrocycle. The Zn-3d shell remains almost unperturbed in the low-energy region of the electronic spectrum.

Of the occupied π levels, the two a_{2u} MOs merit special attention in view of their importance for the excitation spectra. In a detailed theoretical study of the ground- and excited-state properties of [PcZn],[22b] it was pointed out that of the two highest lying occupied a_{2u} MOs, the actual Gouterman orbital is the lowest one, viz. the $1a_{2u}$ in [PcZn] level scheme of Figure 3, which has a large amplitude on the aza bridges and pyrrolic nitrogens. This also holds true for [TTDPzZn], as inferred from Figure 3, where the plot of the $1a_{2u}$ is displayed for both complexes. The higher lying $2a_{2u}$ has very little N_b-$2p_z$ character in both [PcZn] and [TTDPzZn] but rather it has a large amplitude on the C_β-$2p_z$ and C_m-$2p_z$ ([PcZn]) or S-$3p_z$ ([TTDPzZn]). The large stabilization (1.10 eV) of the two lowest unoccupied $1e_g$* Gouterman MOs upon replacement of the benzo rings by thiadiazole rings is consistent with the experimental electrochemical data which show the first reduction potential to shift anodically by 0.63 V (vs SCE) upon going from [PcZn] to the Zn^{II} thiadiazole analog (see the sequence of potentials given above). It is worth noting that, due to differential stabilization of the HOMO and LUMO (1.21 vs 1.10 eV), the HOMO−LUMO gap in [TTDPzZn] is larger than in [PcZn]. As will be discussed later, the increased HOMO−LUMO gap is at the origin of the observed blue shift of the Q band when moving from phthalocyanines to thiadiazoleporphyrazines. Moreover, in both Zn^{II} complexes the annulated groups introduce in the virtual spectrum a set of low-lying π* levels. In [TTDPzZn] this set comprises the $2b_{2u}$, $3a_{2u}$, and $2e_g$*, the lowest of which, the $2b_{2u}$, is located ∼0.8 eV above the unoccupied Gouterman MOs. The large amplitude of these MOs on the annulated thiadiazole groups is evident in the plot of the $2b_{2u}$, displayed in Figure 3. In [PcZn] the analogous π* levels are located at much higher energy to enter the diagram of Figure 3. Noticeably, the lowest MO of the set, the $2b_{2u}$, lies ∼1.4 eV above the LUMO.

(28) Mack, J.; Stillman, M. J. *J. Phys. Chem.* **1995**, *99*, 7935, and references therein.
(29) Nguyen, K. A.; Pachter, R. *J. Chem. Phys.* **2001**, *114*, 10757.

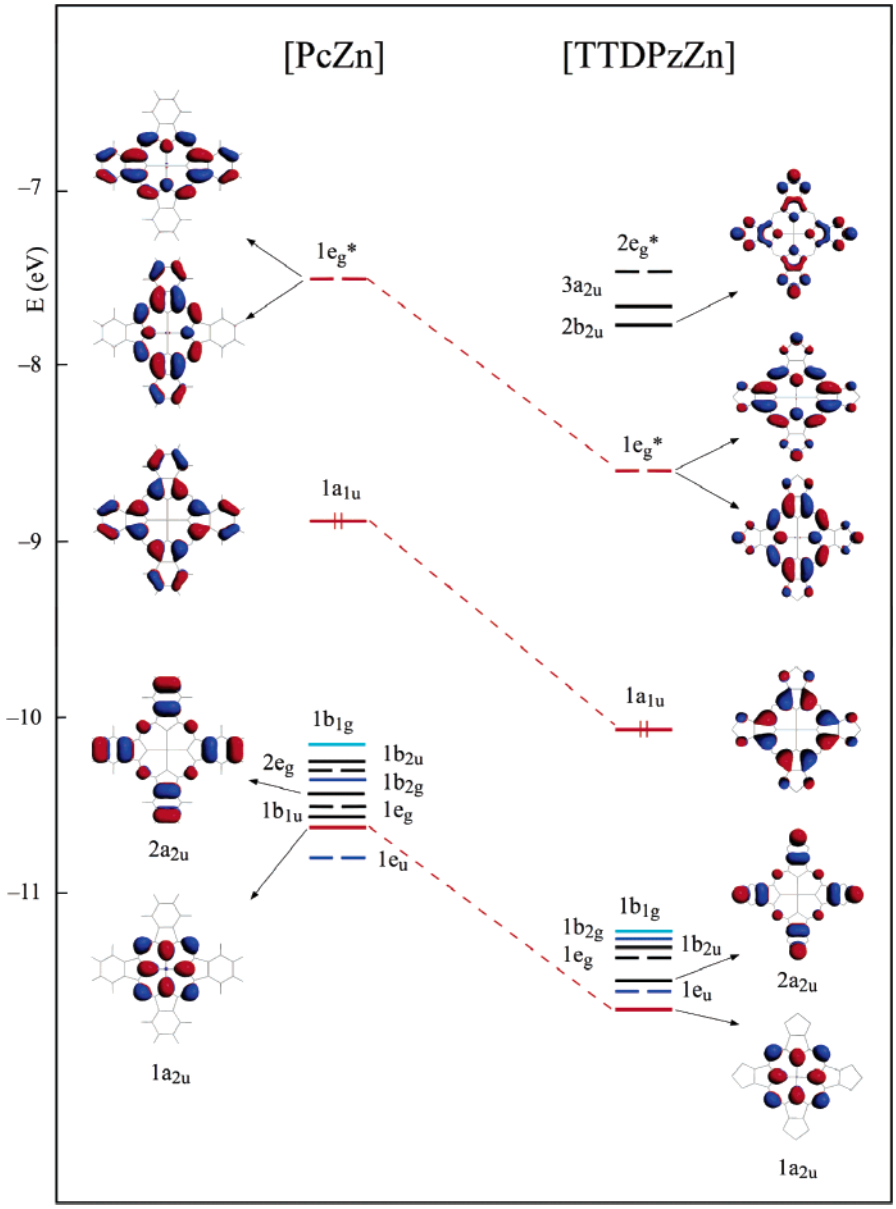

Figure 3. DFT-SAOP ground-state molecular orbital description of [PcZn] and [TTDPzZn]. In the numbering of the MOs the inner electrons are not included. The Gouterman a_{1u}, a_{2u}, and e_g* MOs are indicated with red lines. The N_p and N_b lone pair MOs are indicated with turquoise green and blue lines, respectively.

As inferred from the level diagram of Figure 4, the salient features of the electronic structure of the thiadiazole porphyrazine macrocycle remain substantially the same when replacing Zn^{II} by Mg^{II}. The only electronic structure changes worth noting are as follows: (i) a large stabilization of the $1b_{1g}$—which is no longer the HOMO-1 in [TTDPzMg]—due to the fact that the Mg-$3d_{x^2-y^2}$ is at too high an energy to interact with the N_p lone pairs and (ii) a modest destabilization of all other MOs resulting from the increased electronic density on the macrocycle because of a less effective charge donation into the metal. According to the Hirshfeld charge analysis, the positive charge on the metal increases from 0.44 to 0.60 when moving from [TTDPzZn] to [TTDPzMg].

Due to the D_{4h}→D_{2h} symmetry lowering, the degenerate levels of e_g and e_u symmetry are split in [TTDPzH$_2$]. As in the chosen coordinate system, the inner H atoms lie on the *x*-axis, the *xz*-component of the e_g levels (b_{2g} in D_{2h} symmetry) is stabilized, and the *yz*-component (b_{3g} in D_{2h}) is destabilized. The same holds for the *x*- and *y*-components of the e_u levels (b_{3u} and b_{2u} in D_{2h}, respectively).

Coming now to the ground-state electronic structure of [TTDPzCu], an appropriate description requires the spin unrestricted formalism, which allows the majority spin (spin up, α) and minority spin (spin down, *β*) to have different energies and orbital description (i.e., one-electron orbitals). Figure 5 provides the unrestricted DFT-SAOP ground-state orbital description of [TTDPzCu]. As expected, the highly delocalized ligand orbitals see little exchange effect, and the splitting between the α- and *β*-components is almost negligible. In contrast, the molecular orbitals that are largely localized on the metal show sizable splitting. This is the case of the Cu−N_p *σ* antibonding $1b_{1g}$. The spin-up and spin-down components, both having sizable Cu-$3d_{x^2-y^2}$ character, i.e., 34% the former, 44% the latter, are separated by an

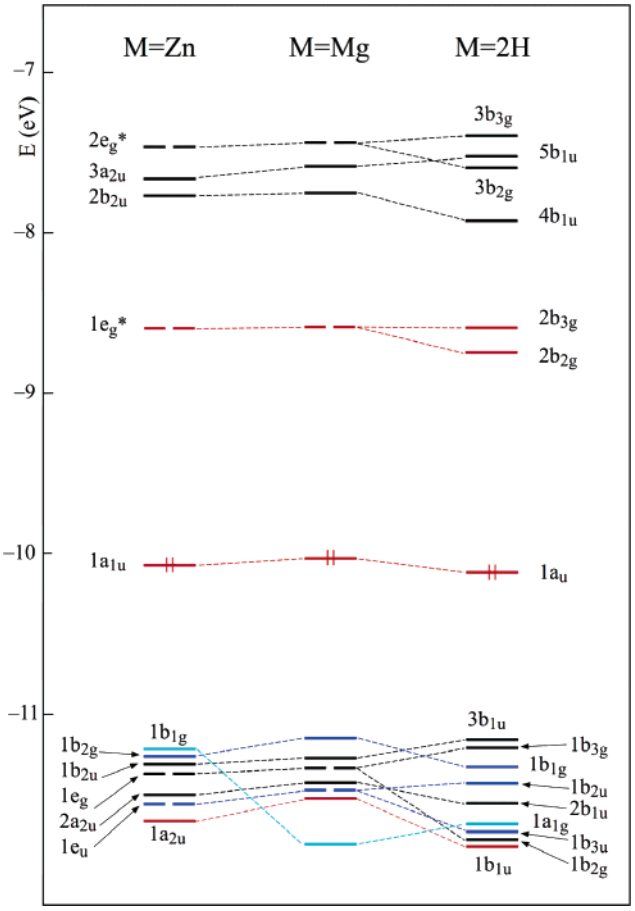

Figure 4. DFT-SAOP ground-state molecular orbital description of [TTDPzZn], [TTDPzMg], and [TTDPzH$_2$]. In the numbering of the MOs the inner electrons are not included. The Gouterman MOs are indicated with red lines. The N_p and N_b lone pair MOs are indicated with turquoise green and blue lines, respectively.

energy gap of ∼0.9 eV. It is worth noting that the lower lying spin-up component, where the Cu-3d unpaired electron resides, lies just below the two nearly degenerate α- and β-spin components of the $1a_{1u}$. This is at variance with [PcCu], for which DFT calculations[30] locate both the α- and β-spin components of the Cu−N_p σ antibonding $1b_{1g}$ MO well above the $1a_{1u}$-HOMO. That the α-spin component of the $1b_{1g}$ lies at lower energy in [TTDPzCu] than in [PcCu] fits with the Cu−N_p bond length being in the former compound ∼0.03 Å longer[27b] than in the latter.[31] Because of the longer Cu−N_p distance, the σ interaction between the Cu-3d$_{x^2-y^2}$ and the N_p lone pairs is weaker in [TTDPzCu] and the Cu−N_p antibonding $1b_{1g}$ is less destabilized than in [PcCu]. Still, the σ interaction between the Cu-3d$_{x^2-y^2}$ and the N_p lone pairs is quite strong in [TTDPzCu], as inferred from the large charge transfer (∼0.6 e) occurring from the macrocycle into the Cu-3d$_{x^2-y^2}$. Actually, this is the strongest metal−macrocycle interaction in the complex. Indeed, the remaining Cu-3d orbitals, the 3d$_{z^2}$ and the 3d$_{xy}$, are almost pure metal states, while the 3d$_\pi$ interacts to some extent with the N_p-2p$_z$. These metal states are located at too low energy to enter the diagram of Figure 5 (the 3d$_{z^2}\beta$, which is the highest lying metal state, is located at −12.88 eV).

(30) Rosa, A.; Baerends, E. J. *Inorg. Chem.* **1994**, *33*, 584.
(31) Brown, C. J. *J. Chem. Soc. A* **1968**, 2488.

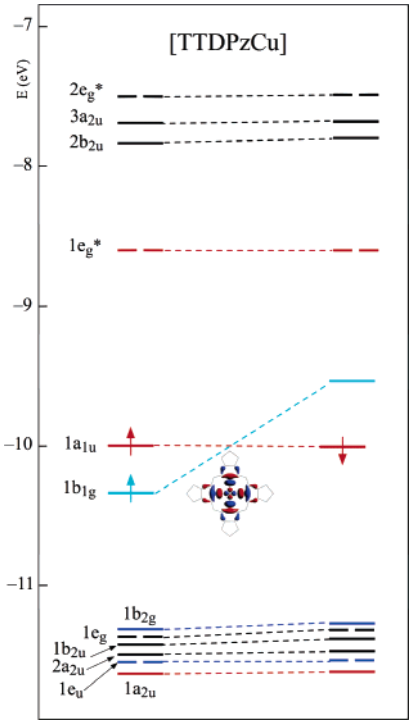

Figure 5. Unrestricted DFT-SAOP ground-state molecular orbital description of [TTDPzCu]. In the numbering of the MOs the inner electrons are not included. The Gouterman a_{1u}, a_{2u}, and e_g* MOs are indicated with red lines. The N_b lone pair MOs are indicated with blue lines. The Cu-3d$_{x^2-y^2}$-N_p lone pair antibonding $1b_{1g}$ (α- and β-components) is indicated with turquoise green lines.

Inclusion of solvation effects leads to a generalized upshift of the highest occupied and lowest unoccupied MOs of [TTDPzH$_2$] and its metal derivatives, as shown in Figure S2 where a comparison of the molecular orbital energies in vacuo and in pyridine is illustrated for the representative case of [TTDPzZn]. While the HOMO-1, HOMO, and the set of unoccupied MOs shown in Figures 3−5 are all destabilized by ∼0.5 eV with respect to their "in vacuo" counterparts, the lowest occupied MOs undergo differential destabilization. As a result, the level ordering in the low-energy region of the electronic spectrum changes with respect to the gas phase and from one compound to another. For instance, in [TTDPzZn] the N_b lone pair $1e_u$ and the Gouterman $1a_{2u}$ MOs appear in the reversed order in pyridine (see level scheme of Figure S2).

Axial ligation of a solvent molecule has little impact on the energy and composition of the "solvated" MOs of either the Mg^{II} or Zn^{II} complexes. When comparing the level schemes of [TTDPzZn] and [TTDPzZn(py)] in pyridine (Figure S2), it is apparent that axial ligation of the pyridine molecule induces, apart from a very small splitting of the e_g and e_u levels due to the D_{4h}→C_{2v} symmetry lowering, only a modest (less than 0.2 eV) upshift of the unsplit orbitals lying below the HOMO-1. This latter is instead slightly stabilized because of the elongation of the Zn−N_p distance upon axial coordination.

With regard to the impact on the optical spectra of the electronic structure changes induced by bulk and specific solvent effects, the above analysis suggests that the inclusion of solvent effects is important to properly account for the

Table 3. Energies (eV) of the LUMO for [TTDPzM] (M = Mg^{II}, Mg^{II}(py), Zn^{II}, Zn^{II}(py), Cu^{II}, $2H^{I}$) and $[TTDPz]^{2-}$ as Obtained from DFT/SAOP Calculations in Pyridine Solution by Using the COSMO Model[a]

	[TTDPzM] M =						
	Mg^{II}	Mg^{II}(py)	Zn^{II}	Zn^{II}(py)	Cu^{II}	$2H^{I}$	$[TTDPz]^{2-}$
LUMO	−8.11 (−8.58)	−8.06	−8.11 (−8.60)	−8.08	−8.15[b] (−8.60[b])	−8.31 (−8.74)	−6.96

[a] The gas-phase values are given in parentheses. [b] The value refers to the α-spin component of the $1e_g$*.

spectral features, particularly for those appearing in the B band region. These arise from transitions out of the MOs lying below the HOMO-1, which are the most altered ones upon solvation.

Electrochemistry. The trend in the first reduction potentials of the currently investigated thiadiazoleporphyrazines can be rationalized in terms of a variation of the LUMO energies along the series, although there is no correspondence in an absolute sense between the LUMO energy value and the first reduction potential. Explicit calculations of the redox potentials to be compared to the experimental electrochemical data will be reported in a forthcoming paper dealing with the spectroelectrochemistry of the title complexes.[32] Table 3 lists the LUMO energies calculated in the gas phase and in pyridine for [TTDPzM] (M = Mg^{II}, Zn^{II}, Cu^{II}, $2H^{I}$), together with values calculated in pyridine for the ligated species, [TTDPzMg(py)] and [TTDPzZn(py)], and for the free-base dianion, $[TTDPz]^{2-}$. As inferred from the data in Table 3, the gas-phase LUMO energies nicely correlate with the first reduction potentials. Indeed they become more negative in the same order as the first reduction potential become less cathodic, i.e., $Mg^{II} < Zn^{II} < Cu^{II} < 2H^{I}$. Upon inclusion of the solvent effects, the LUMO energies rise by ∼0.5 eV with respect to the "in vacuo" values so that, in pyridine, the LUMO energies show substantially the same trend as in vacuo. The first reduction sequence is still reproduced theoretically if the Zn^{II} and Mg^{II} complexes were mostly present in the axially ligated form, as axial ligation has only negligible, if any, effect on the LUMO energies. DFT calculations strongly support the above assumption that in pyridine it is the neutral species $[TTDPzH_2]$ being reduced instead of $[TTDPz]^{2-}$. Indeed, Table 3 shows that the LUMO energy for the neutral form of the free-base compound is 1.35 eV more negative than that of the dianion, suggesting that the former species should be reduced much more easily than the latter.

Optical Spectra. The electronic absorption spectra of the Zn^{II}, Mg^{II}, and Cu^{II} complexes in pyridine are shown in Figure 6. The visible region is dominated by a relatively intense Q band centered in all complexes at about 640 nm showing vibrational structure. The near-UV region of the spectrum is characterized by a rather broad band at ca. 330 nm denoted as B,[12] and there are also two discernible features to the red, the intensity and position of which vary slightly from one metal complex to another.

(32) Donzello, M. P.; Ercolani, C.; Kadish, K. M.; Ricciardi, G.; Rosa, A., manuscript to be submitted.

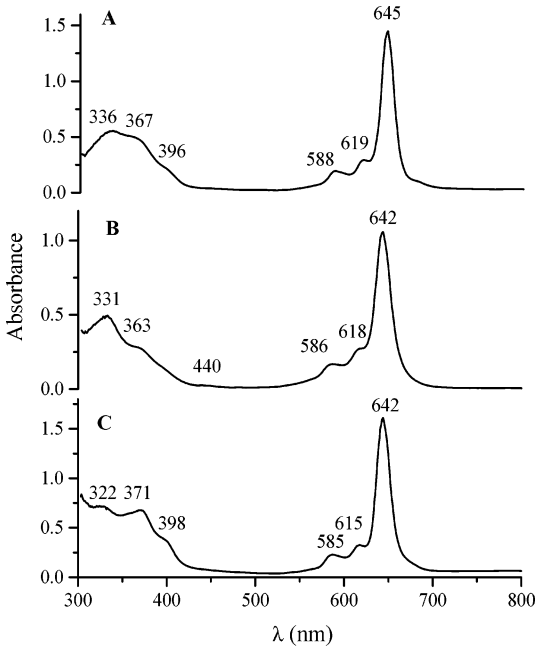

Figure 6. UV−visible spectra in pyridine of [TTDPzZn] (A), [TTDPzCu] (B), and $[TTDPzMg(H_2O)]$ (C).

Table 4. Calculated Excitation Energies, *E* (nm), and Oscillator Strengths (*f*) for the Lowest Optically Allowed Excited States of [TTDPzZn] and [TTDPzMg] in Pyridine Compared to the Experimental Data[a,b]

	TDDFT			
state	composition (%)	*E*	*f*	expt[c] λ_{max}/nm
	[TTDPzZn]			
1^1E_u	$1a_{1u} \rightarrow 1e_g^*$ (86)	608	0.399	645 (Q)
4^1E_u	$2a_{2u} \rightarrow 1e_g^*$ (90)	427	0.123	396
5^1E_u	$1e_g \rightarrow 2b_{2u}$ (58) $1e_g \rightarrow 3a_{2u}$ (26) $1a_{2u} \rightarrow 1e_g^*$ (11)	354	0.263	367
6^1E_u	$1a_{2u} \rightarrow 1e_g^*$ (29) $1e_g \rightarrow 3a_{2u}$ (37) $1b_{2u} \rightarrow 2e_g^*$ (24)	340	0.749	336 (B)
7^1E_u	$1a_{2u} \rightarrow 1e_g^*$ (36) $1e_g \rightarrow 2b_{2u}$ (16) $1b_{2u} \rightarrow 2e_g^*$ (25)	340	0.480	
	[TTDPzMg]			
1^1E_u	$1a_{1u} \rightarrow 1e_g^*$ (85)	615	0.392	642 (Q)
4^1E_u	$2a_{2u} \rightarrow 1e_g^*$ (89)	431	0.125	398
5^1E_u	$1e_g \rightarrow 2b_{2u}$(46) $1a_{2u} \rightarrow 1e_g^*$ (29) $1e_g \rightarrow 3a_{2u}$ (13)	353	0.703	371
6^1E_u	$1a_{2u} \rightarrow 1e_g^*$ (41) $1e_g \rightarrow 3a_{2u}$(24) $1e_g \rightarrow 2b_{2u}$(18)	343	0.923	322 (B)

[a] The major one-electron transitions contributing to the excited states are also given. [b] Only the excited states with an oscillator strength larger than 0.100 are reported. [c] This work.

The excitation energies and oscillator strengths calculated for the lowest optically allowed E_u states are summarized in Tables 4 and 5, together with the experimental band maxima. The tables also include the composition of the excited states in terms of the one-electron MO transitions. According to our TDDFT results, the Q(0,0) band is assigned, in the case of [TTDPzZn] and [TTDPzMg], to the 1^1E_u state, and in the case of [TTDPzCu] to 2^2E_u state, in fairly good agreement

Table 5. Calculated Excitation Energies, *E* (nm), and Oscillator Strengths (*f*) for the Lowest Optically Allowed Excited States of [TTDPzCu] in Pyridine Compared to the Experimental Data[a,b]

	TDDFT			
state	composition (%)/spin	*E*	*f*	expt[c] λ_{max}/nm
2^2E_u	$1a_{1u} \rightarrow 1e_g^*$ (45)/β $1a_{1u} \rightarrow 1e_g^*$ (41)/α	620	0.315	642 (Q)
9^2E_u	$2a_{2u} \rightarrow 1e_g^*$ (41)/β $2a_{2u} \rightarrow 1e_g^*$ (32)/α $1a_{2u} \rightarrow 1e_g^*$ (15)/β	422	0.110	~440
13^2E_u	$1e_u \rightarrow 1b_{1g}$ (35)/β $1e_g \rightarrow 3a_{2u}$ (19)/β $1e_g \rightarrow 2b_{2u}$ (17)/β	363	0.114	363
17^2E_u	$1b_{2u} \rightarrow 2e_g^*$ (25)/β $1e_u \rightarrow 1b_{1g}$ (15)/β $1a_{2u} \rightarrow 1e_g^*$ (12)/α $1a_{2u} \rightarrow 1e_g^*$ (12)/β	340	0.565	331 (B)

[a] The major one-electron transitions contributing to the excited states are also given. [b] Only the excited states with an oscillator strength larger than 0.100 are reported. [c] This work.

with the experiment. As inferred from their composition, the 1^1E_u and 2^2E_u states mainly originate, just as in the Pc analogues, from the $1a_{1u} \rightarrow 1e_g^*$ Gouterman transition. The increased energy gap between these orbitals in thiadiazole-porphyrazines (see Discussion above) fits in with the observed blue shift of the Q band upon going from the TTDPz to the Pc derivatives.

As inferred from the numbering of the excited states listed in Tables 4 and 5, weak excited states are computed as being to the blue of the Q band. Some of these states (the $2,3^2E_u$ in the case of the Mg^{II} and Zn^{II} derivatives and $3,5,6,7^2E_u$ in the case of Cu^{II}) arise from transitions involving partially localized MOs, so they have some charge-transfer (CT) character. As the Kohn−Sham potential used in the present calculations is not corrected for self-interaction, they are likely to be computed at too low energy, according to the well-known tendency of TDDFT methods using traditional functionals to underestimate CT transitions.[33] Therefore, these states must be considered as "spurious".

In the near-UV region, TDDFT calculations predict at least three excited states of appreciable or high intensity, the lowest of which, the 4^1E_u in [TTDPzMg] and [TTDPzZn], the 9^2E_u in [TTDPzCu], accounts well for the rather weak feature appearing at 398, 396, and ~440 nm in the optical spectra of Mg^{II}, Zn^{II}, and Cu^{II} complexes, respectively. According to the composition of the pertinent excited states, this rather weak absorption mainly originates from the $2a_{2u} \rightarrow 1e_g^*$ $\pi \rightarrow \pi^*$ transition. The ~40 nm red shift of this feature in the Cu^{II} complex relative to the Mg^{II} and Zn^{II} analogues is in line with the $2a_{2u} \rightarrow 1e_g^*$ transition undergoing, in the 9^2E_u state, configuration interaction with the lower lying $1a_{2u} \rightarrow 1e_g^*$ transition. In the copper complex several weak or very weak excited states are predicted in the near-UV region. These states involve transitions from fully occupied orbitals to the singly occupied Cu-$3d_{x^2-y^2}$ orbital.

(33) (a) Dreuw, A.; Head-Gordon, M. *J. Am. Chem. Soc.* **2004**, *126*, 4007. (b) Gritsenko, O.; Baerends, E. J. *J. Chem. Phys.* **2004**, *112*, 655.

Table 6. Calculated Excitation Energies, *E* (nm), and Oscillator Strengths (*f*) for the Lowest Optically Allowed Excited States of $[TTDPz]^{2-}$ in Pyridine and $[TTDPzH_2]$ in PhCl Compared to the Experimental Data[a,b]

	TDDFT			
state	composition (%)	*E*	*f*	expt[c] λ_{max}/nm
	$[TTDPzH_2]$			
1^1B_{2u}	$1a_u \rightarrow 2b_{2g}$ (87)	633 (630)[d]	0.200 (0.203)[d]	653 (Q_y)
1^1B_{3u}	$1a_u \rightarrow 2b_{3g}$ (83)	599 (599)[d]	0.185 (0.184)[d]	641 (Q_x)
4^1B_{3u}	$2b_{1u} \rightarrow 2b_{2g}$ (62) $1b_{1u} \rightarrow 2b_{2g}$ (22)	413	0.256	415 (sh)
5^1B_{3u}	$1b_{1u} \rightarrow 2b_{2g}$ (47) $3b_{1u} \rightarrow 3b_{2g}$ (24) $2b_{1u} \rightarrow 2b_{2g}$ (10) $1a_u \rightarrow 2b_{3g}$ (10)	347	0.629	333 (B)
7^1B_{2u}	$1b_{1u} \rightarrow 2b_{3g}$ (59) $2b_{1u} \rightarrow 2b_{3g}$ (12)	332	0.720	
	$[TTDPz]^{2-}$			
1^1E_u	$1a_{1u} \rightarrow 1e_g^*$(76) $1a_{1u} \rightarrow 2e_g^*$(18)	628	0.247	648 (Q)
2^1E_u	$1a_{1u} \rightarrow 2e_g^*$ (72) $1a_{1u} \rightarrow 1e_g^*$ (16)	505	0.205	483
4^1E_u	$2a_{2u} \rightarrow 1e_g^*$ (38) $1a_{2u} \rightarrow 1e_g^*$ (36)	406	0.100	397 (sh)
5^1E_u	$2a_{2u} \rightarrow 2e_g^*$ (64) $1a_{2u} \rightarrow 1e_g^*$ (25)	375	0.130	375
8^1E_u	$1a_{2u} \rightarrow 2e_g^*$ (23) $2a_{2u} \rightarrow 1e_g^*$ (20) $1a_{2u} \rightarrow 1e_g^*$ (19) $2a_{2u} \rightarrow 2e_g^*$ (16)	342	0.944	318 (B)

[a] The major one-electron transitions contributing to the excited states are also given. [b] Only the excited states with an oscillator strength larger than 0.100 are reported. [c] This work. [d] TDDFT/SAOP data in pyridine.

On the basis of the calculated excitation energies and oscillator strengths, the 5^1E_u state—in the case of the Zn^{II} and Mg^{II} complexes—and the 13^2E_u—in the case of the Cu^{II} complex—are the best candidates for assignment to the next quite intense feature peaking in all systems at about 370 nm (see Figure 6). In the Zn^{II} and Mg^{II} systems this feature has a clear $\pi \rightarrow \pi^*$ character, as the 5^1E_u excited state is in both complexes a mixture of $\pi \rightarrow \pi^*$ transitions, viz., the $1a_{2u} \rightarrow 1e_g^*$, $1e_g \rightarrow 2b_{2u}$, and $1e_g \rightarrow 3a_{2u}$. In the Cu^{II} complex the feature at 370 nm has, instead, a mixed LMCT/ $\pi\pi^*$ character, the $1e_u$ (N_b lone pair)$\rightarrow 1b_{1g}$ ($3d_{x^2-y^2}$) LMCT transition entering in the underlying 13^2E_u excited state with a sizable (35%) weight.

The assignment of the B band is straightforward. TDDFT results in Tables 5 and 6 show that this originates in [TTDPzMg] from the 6^1E_u, in [TTDPzZn] from the $6,7^1E_u$ degenerate pair of excited states, and in [TTDPzCu] from the 13^2E_u. The composition of these states reveals that the B band has a pure (Mg^{II} and Zn^{II}) or predominant (Cu^{II}) $\pi\pi^*$ character, with the $1a_{2u} \rightarrow 1e_g^*$ Gouterman transition entering with a large weight.

TDDFT calculations on the axially ligated Mg^{II} species, [TTDPzMg(py)] and [TTDPzMg(H_2O)] (not reported), show that axial ligation has very little impact, if any, on the calculated energies and intensities of the main spectral features, hence providing nearly the same interpretation of the optical spectra. Thus, on the basis of the calculated

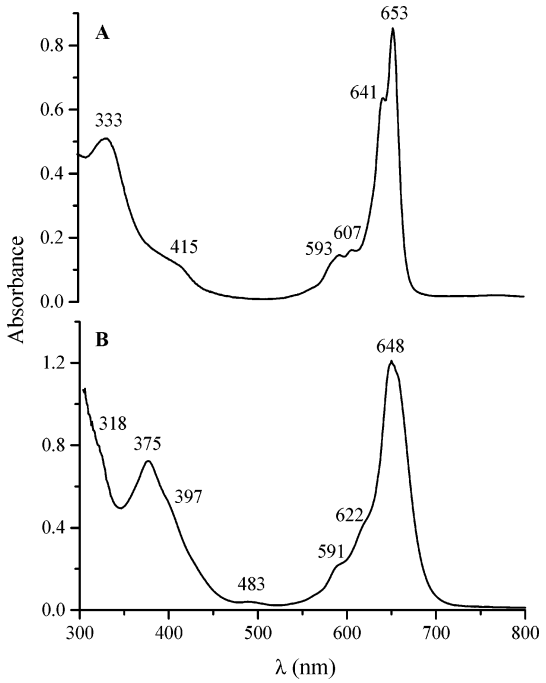

Figure 7. UV−visible spectra of [$TTDPzH_2$] in PhCl (A) and pyridine (B).

spectra it is not possible to discriminate which is the prevailing form of the Mg^{II} complex in pyridine solution. As for the Zn^{II} complex, TDDFT results on the ligated form of the compound, [TTDPzZn(py)], reproduce quite well the Q band main feature but not the near-UV spectral region, where only two nearly degenerate excited states, the 8^1B_1 and 9^1B_2 calculated at 379 and 378 nm, respectively, and with summed oscillator strength of 0.677, are predicted. So, on the basis of TDDFT results, one may conclude that the Zn^{II} complex mainly exists in the unligated form in pyridine solution.

We now come to an interpretation of the spectroscopic behavior of the free-base thiadiazoleporphyrazine. As inferred from Figure 7, the main spectral features of the UV−visible absorption spectrum of [$TTDPzH_2$] show a marked dependence on solvent. While in PhCl the spectral features are those typical of D_{2h} free-base porphyrazines,[12] in pyridine they are consistent with [$TTDPzH_2$] being preponderantly in its deprotonated form, $[TTDPz]^{2-}$.

The excitation energies and oscillator strengths calculated for the lowest excited states of [$TTDPzH_2$] in PhCl (see Table 6) satisfactorily account for the main spectral features. The two components of the Q band at 653 and 641 nm are assigned to the 1^1B_{2u} and 1^1B_{3u} excited states calculated at 633 and 599 nm and with oscillator strength of 0.200 and 0.185, respectively. The energies of the Q bands and their relative intensities are well reproduced theoretically, although the computed splitting of 34 nm is somewhat larger than the experimental value (12 nm in PhCl). At variance with [PcH_2], for which both SAC-CI (Symmetry Adapted Cluster-Configuration Interaction)[34] and TDDFT/SAOP[35] calculations predict the lower energy Q band to be polarized along the H−H axis (Q_x), the lower energy Q band of [$TTDPzH_2$] is predicted to be polarized perpendicular to the H−H axis (*x*-axis in Chart 2) and, accordingly, is denoted as Q_y in Table 6. No excited states of appreciable intensity are calculated up to ~500 nm, confirming that the relatively weak features to the blue of the Q band main components are vibrational in origin. We note, in passing, that the weak $2,3^1B_{2u}/^1B_{3u}$ and the 4^1B_{2u} excited states computed to the blue of the Q bands must be considered as "spurious" states for the reasons discussed above.

In the energy regime of the Soret band, three excited states are predicted, the 4^1B_{3u}, 5^1B_{3u}, and 7^1B_{2u}. Of these, the moderately intense 4^1B_{3u} calculated at 413 nm is responsible for the shoulder appearing in the red tail of the B band, at 415 nm, whereas the pair of intense 5^1B_{3u} and 7^1B_{2u} excited states calculated at 347 and 332 nm account for the B band centered at 333 nm. The computed splitting (15 nm) between the *x*- (B_{3u}) and *y*- (B_{2u}) components of the B band is in line with the rather broad profile of this band. As inferred from the composition of the pertinent excited states, both the *x*- and *y*-components of the B band largely arise from the $1b_{1u} \rightarrow 2b_{3g}$ and $1b_{1u} \rightarrow 2b_{2g}$ Gouterman transition, respectively. A split Q band is also predicted when the optical spectrum of [$TTDPzH_2$] is computed in pyridine solution (see Table 6) suggesting that the coalescence of the Q bands observed in this solvent is not merely due to bulk solvent effects. This seems to support the view that the species responsible for the spectrum in pyridine (Figure 6B) is the deprotonated form of the free-base, $[TTDPz]^{2-}$. As can be inferred from Table 6, the excitation energies and oscillator strengths calculated for the lowest excited states of the dianion nicely reproduce the salient features of the optical spectrum of [$TTDPzH_2$] in pyridine, fully confirming this view.

Conclusions

The cyclic voltammetric behavior of tetrakis(thiadiazole)-porphyrazines having the formula [TTDPzM] (M = Mg^{II}-(H_2O), Zn^{II}, Cu^{II}, $2H^{I}$) were examined in different basic and low-donor media (pyridine, DMSO, and DMF). The ground- and excited-state electronic properties of these compounds were studied in detail by DFT/TDDFT methods, taking into account bulk solvent effects. For the Mg^{II} and Zn^{II} complexes the energetics of the formation of the axially ligated [TTDPzM(py)] species in pyridine solution was investigated, and it is found that both complexes may exist in this solvent also in the ligated form.

Stepwise well-separated nicely reversible ligand-centered one-electron reductions appear in the potential range of 0.0 to −2.0 V vs SCE, but no redox processes are observed at positive potentials. Due to the electron-withdrawing effect of the externally annulated thiadiazole rings, the measured $E_{1/2}$ values are for all the species remarkably less negative than the corresponding reduction potentials for their phthalocyanine analogues. This behavior is explained on the basis of the ground-state electronic structure calculations which reveal that replacement of the benzo rings by thiadiazole rings induces a large stabilization of both the HOMO and

(34) Toyota, K.; Hasegawa, J.; Nkatsuji, H. *J. Phys. Chem. A* **1997**, *101*, 446.
(35) Rosa, A.; Ricciardi, G., unpublished results.

LUMOs. The first one-electron reduction potentials of the [TTDPzM] species are found to nicely correlate with the gas-phase LUMO energies along the series. The first reduction sequence for the [TTDPzM] compounds is still theoretically reproduced in pyridine, even if the Zn^{II} and Mg^{II} complexes are assumed to be in their axially ligated form. TDDFT calculations of the lowest excited states have been performed for the Zn^{II}, Mg^{II}, and Cu^{II} complexes as well as for the pentacoordinated monoadducts [TTDPzMg(py)] and [TTDPzZn(py)], using pyridine as solvent. The calculations provide an accurate and unambiguous description of the UV−visible spectra. The calculated optical spectra, while indicating that the Zn^{II} complex mainly exists in its unligated form in pyridine solution, do not allow to discriminate as to which is the prevailing form of the Mg^{II} complex, ligated or unligated, in this solvent.

The calculated optical spectra for the free-base [$TTDPzH_2$] in PhCl and pyridine confirm previous experimental data in that the prevalent form present in pyridine is the dianion $[TTDPz]^{2-}$. DFT results, in line with the electrochemical data, indicate, however, that in pyridine it is the neutral species [$TTDPzH_2$] being reduced instead of the compound in its deprotonated form $[TTDPz]^{2-}$.

Acknowledgment. Financial support by the University of Rome "La Sapienza" and the MIUR (C.E.) and the Robert A. Welch Foundation (K.M.K, Grant E-680) is gratefully acknowledged. M. P. Donzello expresses her gratitude to the Department of Chemistry, Houston University, for kind hospitality.

Supporting Information Available: Cyclic voltammograms, with added $E_{1/2}$ values of [TTDPzCu], [TTDPzMg(H_2O)], [TTDPzZn], and [$TTDPzH_2$] in DMSO (Figure S1); DFT-SAOP ground-state molecular orbital description of [TTDPzZn] in the gas phase and [TTDPzZn] and [TTDPzZn(py)] in pyridine (Figure S2); and selected bond distances (Å) and bond angles (deg) calculated for [TTDPzM] (M = Mg^{II}, Zn^{II}, Cu^{II}) and for $[TTDPz]^{2-}$ in pyridine (Table S1). This material is available free of charge via the Internet at http://pubs.acs.org.

IC070038D